Asymmetrical Wall Baffles to Assist Upstream Fish Passage in Box Culvert: Physical Modeling

Xinqian Leng[1] and Hubert Chanson[2]

Abstract: Although waterway connectivity is a requirement for all freshwater fish, culverts have had negative impacts on freshwater river ecology. Following a recent biological study suggesting that asymmetrical wall baffles may be conducive to upstream passage of small-bodied fish, experimental modeling of plain wall baffles on one sidewall only was conducted under controlled flow conditions. The measurements were performed in a 15-m-long, 0.5-m-wide culvert barrel channel at several longitudinal and transverse locations for a broad range of discharges and baffle geometries to deliver a fine characterization of the hydrodynamics of the asymmetrically baffled channel. The physical modeling data illustrated the drastic impact of a seemingly simple boundary treatment (i.e., plain rectangular baffles) on the flow field. In practice, the installation of baffles has practical engineering implications that must not be ignored. **DOI: 10.1061/(ASCE)IR.1943-4774.0001514.**

Author keywords: Box culverts; Asymmetrical sidewall baffles; Flow resistance; Recirculation; Fish passage; Physical modeling.

Introduction

Unimpeded waterway connectivity is a requirement for all freshwater fish. Barriers to fish movement can lead to population fragmentation and decline even in nonmigratory species (Dynesius and Nilsson 1994). Although culverts are common yet important structures in relation to transportation and hydrological control, they have negative impacts on freshwater river ecology, including small-body-mass native fish species and juvenile of larger fish (Behlke et al. 1991; Kemp 2012). Common issues hindering fish passage include excessive water velocity in the culvert barrel, shallow flow depths, excessive vertical drop at the outlet lip (perched outlet), and blockage from debris accumulation in the structure inlet and barrel (Olsen and Tullis 2013; Chanson and Leng 2021).

For culvert retrofitting as well as new designs, baffles may be installed along the culvert barrel to provide some fish-friendly alternative (Olsen and Tullis 2013; Duguay and Lacey 2014) (Fig. 1). For low discharges, the baffles decrease the flow velocity and increase the water depth to facilitate fish passage while offering rest areas (Cahoon et al. 2007). At larger discharges, baffles induce lower local velocities and generate recirculation regions, and they can reduce drastically the culvert discharge capacity for a given afflux (Larinier 2002; Olsen and Tullis 2013), thus increasing substantially the total cost of the structure to achieve the same design discharge and afflux. Various baffle designs have been proposed. Many have been mostly bottom-mounted (Larinier 2002; Cahoon et al. 2007; Olsen and Tullis 2013), as illustrated in Fig. 1(b). A few sidewall-mounted designs have been proposed (Kapitzke 2010; Marsden 2015), as seen in Fig. 1(b). Recently, smaller bottom-corner baffles were proposed (Cabonce et al. 2018, 2019). In addition to the mounting, the baffle designs were often symmetrically installed about the channel centerline. A few recent studies discussed the importance of asymmetrical placement to enhance secondary flows and enlarge low-velocity zones (Olsen and Tullis 2013; Cabonce et al. 2019).

A recent biological study suggested that asymmetrical wall baffles may be conducive of upstream passage of small-bodied Australian native fish and juveniles of large fish (Marsden 2015). Herein, physical modeling of full-height plain wall baffles on one sidewall only was conducted under controlled flow conditions in a relatively large rectangular barrel channel. The measurements delivered a fine characterization of the hydrodynamics of the asymmetrically baffled channel, acting as a full-scale box culvert barrel. The results lead to a detailed quantitative hydrodynamic assessment of the impact of full-height sidewall baffles on the box culvert.

Physical Modeling and Experimental Conditions

Dimensional Considerations

An experimental investigation is expected to deliver a sound prediction of the flow properties in a hydraulic structure (Henderson 1966). The modeling approach must be based upon the fundamental principles of similitude. Dimensional analysis is the relevant methodology to deliver the key relevant properties (Rouse 1938; Chanson 2004). In a study of channel flow past baffles, the relevant dimensional variables include the fluid and physical properties, channel geometry, baffle dimensions, and inflow conditions. For a steady turbulent flow in a rectangular asymmetrical channel with full-height sidewall baffles (Fig. 2), a dimensional analysis yields a series of dimensionless relationships in terms of the steady flow field at a location (x, y, z)

[1]Research Fellow, School of Civil Engineering, Univ. of Queensland, Brisbane, QLD 4072, Australia; presently, Research Fellow, Université de Bordeaux, I2M, Laboratoire Transfert Fluide Énergétique, Pessac 33607, France.

[2]Professor in Hydraulic Engineering, School of Civil Engineering, Univ. of Queensland, Brisbane, QLD 4072, Australia (corresponding author). ORCID: https://orcid.org/0000-0002-2016-9650. Email: h.chanson@uq.edu.au

Note. This manuscript was submitted on February 1, 2020; approved on July 24, 2020; published online on September 23, 2020. Discussion period open until February 23, 2021; separate discussions must be submitted for individual papers. This paper is part of the ***Journal of Irrigation and Drainage Engineering***, © ASCE, ISSN 0733-9437.

(a)

(b)

Fig. 1. Box culverts equipped with baffles in eastern Australia: (a) culvert beneath Paradise Road, Slacks Creek, Queensland, Australia, on June 6, 2019, low flow in the cell equipped with bottom baffles (0.20 m high, 5 m apart in the longitudinal direction); and (b) culvert beneath Discovery Road, Townsville, Queensland, Australia, on November 15, 2019 with sidewall baffles on the left.

$$\frac{d}{d_c}, \frac{V_x}{V_c}, \frac{P}{\rho \times g \times d_c}, \frac{L_t}{d_c}, T_t \times \sqrt{\frac{g}{d_c}}, \ldots = F\left(\begin{array}{l} \frac{x}{d_c}, \frac{y}{d_c}, \frac{z}{d_c} \\ \frac{B}{d_c}, \theta, \frac{k_s}{D_H}, \frac{B}{h_b}, \frac{L_b}{h_b} \\ \frac{d_1}{d_c}, \frac{V_1}{\sqrt{g \times d_1}} \\ \rho \times \frac{V \times D_H}{\mu}, \frac{g \times \mu^4}{\rho \times \sigma^3}, \ldots \end{array}\right) \quad (1)$$

where d = flow depth; V_x = longitudinal velocity component; P = local pressure; L_t = local turbulent length scale; T_t = turbulent time scale; g = gravity acceleration; d_c and V_c = critical depth and velocity, respectively; x, y, and z = longitudinal, transverse, and vertical coordinates, respectively; B = channel width; k_s = equivalent sand roughness height of the channel boundary; D_H = hydraulic diameter; h_b = baffle protuberance relative to the sidewall [Fig. 2(a)]; L_b = longitudinal spacing between baffles; θ = angle between the bed and horizontal; d_1 = inflow depth; V_1 = inflow velocity; ρ = water density; μ = water dynamic viscosity; and σ = surface tension. Implicitly, Eq. (1) assumes a constant baffle size and spacing along the entire rectangular channel.

In Eq. (1)'s right-hand side, the 10th, 11th, and 12th terms are the inflow Froude number Fr_1, Reynolds number Re, and Morton number Mo, respectively. When an open-channel-flow study is undertaken with air and water in both laboratory and prototype channels, the Morton number is an invariant, thus simplifying Eq. (1). Considering the flow in an asymmetrical rectangular channel (Fig. 2), the preceding analysis shows the large number of relevant parameters. A true similarity would require all dimensionless variables to be identical, including Froude, Reynolds, and Morton numbers, in the laboratory and prototype. Such a true similarity is physically impossible. In the current study, the experiments were conducted in a near-full-scale facility operating at relatively large Reynolds numbers: $0.96 \times 10^5 < Re < 4.5 \times 10^5$. Any extrapolation of the results should be based upon a Froude and Morton similarity.

Experimental Channel and Instrumentation

The investigation was conducted in a 15-m-long, 0.4-m-high, and 0.5-m-wide ($B = 0.50$ m) tilting flume. The bed and sidewalls of the flume were made of PVC and glass, respectively. The bed of the channel was horizontal, i.e., $\theta = 0$, in turn simplifying Eq. (1). Water was delivered to the flume through a 2.0-m-long, 1.25-m-wide intake structure equipped with baffles, flow straighteners, and three-dimensional convergent, and was supplied by a constant-head reticulation system. The intake structure was designed to deliver smooth inflow conditions, and the constant-head reservoir enabled a well-controlled constant flow rate. At the downstream end, the flume ended with a free overfall.

Several boundary conditions were tested: (1) smooth channel without baffle; (2) small plain baffles $h_b = 0.042$ m; (3) medium baffles $h_b = 0.083$ m; and (4) large baffles $h_b = 0.167$ m. The smooth channel was used as the reference configuration. The plain baffles were full-height rectangular sidewall baffles made of 6-mm-thick PVC sheets cut with a water-jet machine with tolerances of less than 0.2 mm. Each baffle was fixed to the floor, held at the top, and sealed to the right sidewall. Further details were reported by Leng and Chanson (2019).

The water discharge was measured with a Venturi meter located on the water supply line. A pointer gauge was utilised to measure the free surface elevation. A Prandtl-Pitot tube was utilized to measure the velocity and pressure in the water. The Pitot tube was a Dwyer 166 Series tube (Dwyer Instruments, Michigan City, Indiana) (Ø3.18 mm) with a hemispherical total head tapping (Ø = 1.19 mm) at the tip and four equally spaced static head tappings (Ø = 0.51 mm) located 25.4 mm behind the tip. The Prandtl-Pitot tube was further used to determine the shear stress at a boundary, i.e., the skin friction, when the tube is in contact with the wall (Preston 1954; Patel 1965). Based upon dimensional and theoretical considerations, the concept was used in the present study following Cabonce et al. (2019). The vertical translation of the Prandtl-Pitot tube was controlled by a fine adjustment traveling mechanism connected to a HAFCO digital scale unit (Kewdale, Western Australia). The experiments were further documented with

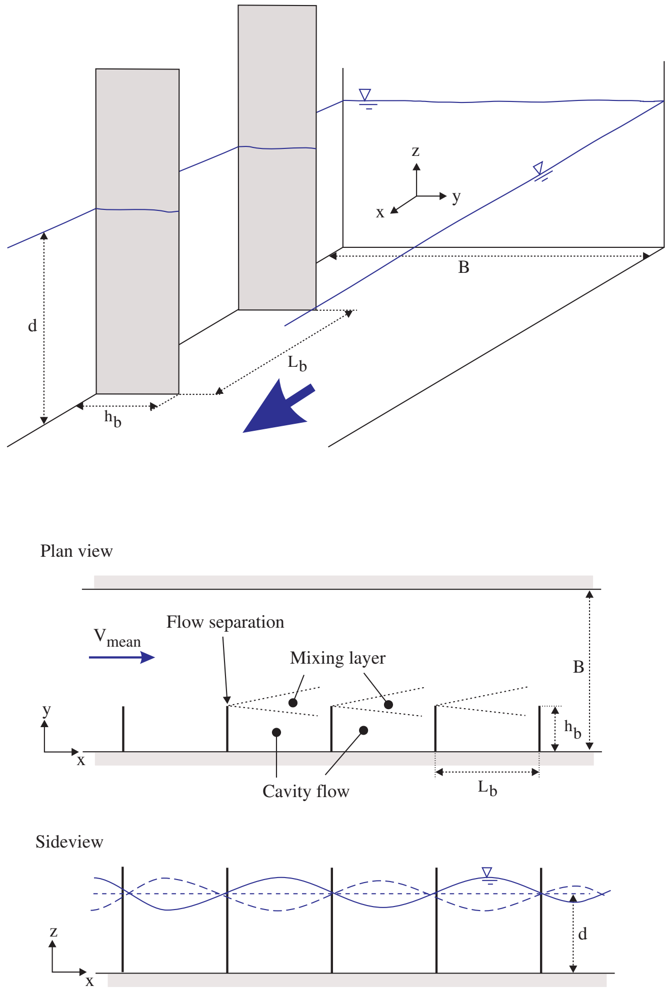

Fig. 2. Sketch of box culvert barrel equipped with full-height sidewall baffles along the right sidewall.

a digital single-lens reflex (dSLR) camera (Pentax K-7, Tokyo) and a digital camera (Casio Exilim EX-10, Tokyo).

Experimental Boundary and Flow Conditions

The experiments were performed in the horizontal channel, acting as a near-full-scale box culvert barrel, for a wide range of water discharges (Table 1). Basic flow pattern observations and free-surface measurements were conducted along the whole length of the flume for flow rates within $0.016\ \mathrm{m}^3/\mathrm{s} < Q < 0.12\ \mathrm{m}^3/\mathrm{s}$, with all baffle sizes, $h_b = 0.042$, 0.083, and 0.167 m, and longitudinal baffle spacing L_b between 0.33 and 1.67 m (Table 1). All tests were conducted with full-height rectangular sidewall baffles installed along the right wall only, and a constant baffle size and spacing was used for each configuration. Detailed velocity measurements were undertaken for one flow rate, $Q = 0.0556\ \mathrm{m}^3/\mathrm{s}$, and one geometry, $h_b = 0.083$ m and $L_b = 0.33$ m.

Measurements were performed in a single wall cavity and repeated for different longitudinal locations $(x - x_b) = 0.0165$, 0.1667, and 0.250 m, as well as at several transversal locations y, where x_b is the longitudinal coordinate of the upstream baffle, $x_b = 8.1$ m, and y is the transversal distance from the right sidewall, positive toward the left sidewall. Each vertical velocity profile consisted of a minimum of 24 points. In addition, boundary shear stress measurements were conducted at each longitudinal location along the entire wetted perimeter using the Prandtl-Pitot tube (Dwyer Instruments, Michigan City, Indiana).

Flow Patterns

Visual observations were conducted using high-definition photographic and video cameras. Typical free-surface flow patterns are presented herein. Overall, the intrusion of the baffles increased significantly the flow turbulence, with visible turbulent structures from the flow surface to underneath the flow. Stagnation was observed as the right side of the flow was brought to rest by a baffle, resulting in a local increase in flow depth and a series of ripples leading up to it [Fig. 3(a)]. Downstream of each baffle, a wake zone was observed, highlighted by some swirling, a small amount of aeration, and a low-velocity zone (LVZ) behind the baffles [Fig. 3(b)]. Some cross waves could be observed on the free surface across the culvert barrel channel [Fig. 3(a), solid arrows]. For the same baffle size and spacing, the flow became visibly more turbulent as the discharge increased, and the free surface became rougher. As the distance between baffles increased, a more turbulent wake zone was created, highlighted by sharper separation around the edge of the baffles, larger decrease in water level before and behind the baffles, and sometimes more aeration in the wake region.

Some free-surface resonance with unstable sloshing was observed for some flow conditions, being more remarkable for higher discharges compared with lower ones. Under such conditions, the water level was not constant and tended to oscillate about its mean value, with some longitudinal sloshing motion in the cavity between two successive baffles, and sometimes across the channel as well. The type of instability patterns was related to the distance between baffles. For the smallest spacing, i.e., $L_b = 0.33$ m, longitudinal sloshing mainly occurred along the right sidewall between baffles. With larger baffle spacings, the free-surface instabilities started to occur more predominately along the left sidewall. Visually the wave length increased with increasing baffle spacing L_b. Fig. 3(f) presents a side view of the channel with some internal longitudinal resonance and Fig. 2 shows a schematic. The self-sustained wave instabilities were not stationary standing waves but pseudoperiodic. Although previous studies of flow structures past a series of cavities (Yossef and De Vriend 2011; Meile et al. 2011; Tuna and Rockwell 2014) focused mostly on the oscillation of the cavities, the self-sustained sloshing motion tended to extend to the entire channel width and length in the current study [Fig. 3(f)].

The transverse oscillations were linked to the asymmetrical channel configuration, and the longitudinal instabilities were caused by large-scale vortices forming from roll-up of the separated mixing layer and interacting with the recirculating flow within the cavity between two baffles. The sloshing instability likely occurred when the instability frequency of the separated shear layer formed at the tip of a baffle matched the natural frequency of the gravity standing wave in the cavity behind the baffle (Tuna and Rockwell 2014). For the flow conditions in Fig. 3(f), the wave amplitude was about $a = 0.036$ m (i.e., $a/d = 0.13$) and the oscillation period was about 1 s. The latter sloshing oscillation period was close to natural sloshing oscillation period for both longitudinal and transverse instability modes, respectively.

Further visualisations of flow patterns were conducted with dye injection into the flow. A low-velocity zone was seen behind the baffles toward the right (baffled) sidewall [Figs. 3(b–e)]. When injected behind the baffle, the dye circulated for a period of time before diffusing and disappearing. The observations indicated the existence of a shear layer between the fast mainstream region and the low-velocity region created by the baffles, and a sizeable

Table 1. Experimental investigation of asymmetrical wall baffles in a box culvert barrel channel (present study)

Geometry	h_b (m)	L_b (m)	Q (m^3/s)	d at $x = 8$ m (m)	V_{mean} at $x = 8$ m (m/s)	Re at $x = 8$ m	f
Smooth	N/A	N/A	0.016	0.072	0.44	9.87×10^4	0.02
	N/A	N/A	0.025	0.09	0.56	1.46×105	0.019
	N/A	N/A	0.035	0.107	0.65	1.95×10^5	0.018
	N/A	N/A	0.056	0.138	0.81	2.87×10^5	0.017
	N/A	N/A	0.098	0.195	1.01	4.37×10^5	0.016
Small baffles	0.042	0.333	0.01789	0.085	0.42	1.06×10^5	0.08
	0.042	0.333	0.0252	0.1	0.50	1.43×10^5	0.065
	0.042	0.333	0.03487	0.123	0.57	1.86×10^5	0.07
	0.042	0.333	0.05676	0.162	0.70	2.74×10^5	0.075
	0.042	0.333	0.1105	0.248	0.89	4.41×10^5	0.075
	0.042	0.667	0.01635	0.073	0.45	1.01×10^5	0.043
	0.042	0.667	0.02791	0.11	0.51	1.54×10^5	0.065
	0.042	0.667	0.03691	0.125	0.59	1.96×10^5	0.054
	0.042	0.667	0.05403	0.161	0.67	2.61×10^5	0.068
	0.042	0.667	0.1038	0.248	0.84	4.14×10^5	0.076
Medium baffles	0.083	0.333	0.0165	0.081	0.41	9.90×10^4	0.08
	0.083	0.333	0.025	0.108	0.46	1.39×10^5	0.095
	0.083	0.333	0.037	0.137	0.54	1.90×10^5	0.1
	0.083	0.333	0.056	0.184	0.61	2.56×10^5	0.12
	0.083	0.333	0.11	0.277	0.79	4.15×10^5	0.15
	0.083	0.667	0.0164	0.086	0.38	9.70×10^4	0.11
	0.083	0.667	0.0252	0.11	0.46	1.39×10^5	0.12
	0.083	0.667	0.0369	0.14	0.53	1.88×10^5	0.14
	0.083	0.667	0.056	0.189	0.59	2.53×10^5	0.16
	0.083	0.667	0.103	0.272	0.76	3.92×10^5	0.2
	0.083	1.333	0.0251	0.118	0.43	1.35×10^5	0.11
	0.083	1.333	0.0367	0.138	0.53	1.88×10^5	0.09
	0.083	1.333	0.0554	0.191	0.58	2.50×10^5	0.12
	0.083	1.333	0.1056	0.295	0.72	3.85×10^5	0.14
Large baffles	0.167	0.333	0.01798	0.106	0.34	1.00×10^5	0.21
	0.167	0.333	0.02576	0.128	0.40	1.35×10^5	0.21
	0.167	0.333	0.03611	0.156	0.46	1.77×10^5	0.22
	0.167	0.333	0.05623	0.205	0.55	2.45×10^5	0.24
	0.167	0.333	0.09588	0.307	0.62	3.42×10^5	0.35
	0.167	0.667	0.01718	0.102	0.34	9.70×10^4	0.225
	0.167	0.667	0.0252	0.131	0.38	1.31×10^5	0.268
	0.167	0.667	0.03651	0.163	0.45	1.76×10^5	0.29
	0.167	0.667	0.05486	0.212	0.52	2.36×10^5	0.3
	0.167	0.667	0.09151	0.287	0.64	3.39×10^5	0.33
	0.167	1	0.01718	0.105	0.33	9.61×10^4	0.22
	0.167	1	0.02631	0.139	0.38	1.34×10^5	0.255
	0.167	1	0.03611	0.167	0.43	1.72×10^5	0.27
	0.167	1	0.05459	0.225	0.49	2.28×10^5	0.36
	0.167	1	0.08381	0.316	0.53	2.94×10^5	0.42
	0.167	1.333	0.019474	0.117	0.33	1.05×10^5	0.21
	0.167	1.333	0.026853	0.141	0.38	1.36×10^5	0.21
	0.167	1.333	0.035284	0.173	0.41	1.66×10^5	0.26
	0.167	1.333	0.054587	0.235	0.46	2.24×10^5	0.28
	0.167	1.333	0.087646	0.32	0.55	3.05×10^5	0.36
	0.167	1.667	0.01798	0.102	0.35	1.01×10^5	0.17
	0.167	1.667	0.02404	0.124	0.39	1.28×10^5	0.22
	0.167	1.667	0.03611	0.159	0.45	1.75×10^5	0.25
	0.167	1.667	0.05318	0.208	0.51	2.31×10^5	0.27
	0.167	1.667	0.08871	0.31	0.57	3.15×10^5	0.33

Note: d = water depth; f = Darcy-Weisbach friction factor; h_b = baffle size measured perpendicular to the right sidewall; L_b = longitudinal baffle spacing; Q = water discharge; Re = Reynolds number defined in terms of the bulk velocity and hydraulic diameter; and V_{mean} = cross-sectional averaged flow velocity positive downstream.

wake region with negative velocities (i.e., recirculation). Figs. 3(b–e) illustrates typical flow structures visualized using dye injection, with the main flow direction from left to right, and solid lines highlighting the trajectories of the dye plume.

Overall, four basic flow patterns were observed during the movements of the dye plume [Figs. 3(b–e)]. Flow pattern 1 happened when the dye was first injected, showing a rotational motion of the dye plume close to the free surface [Fig. 3(b)]. Then, the dye plume started to diffuse and disperse through the entire water column, leading to a downward motion, namely Flow pattern 2 [Fig. 3(c)]. The dye plume then detached into two plumes; one remained close to the free surface and the other sank toward the channel bed (Flow

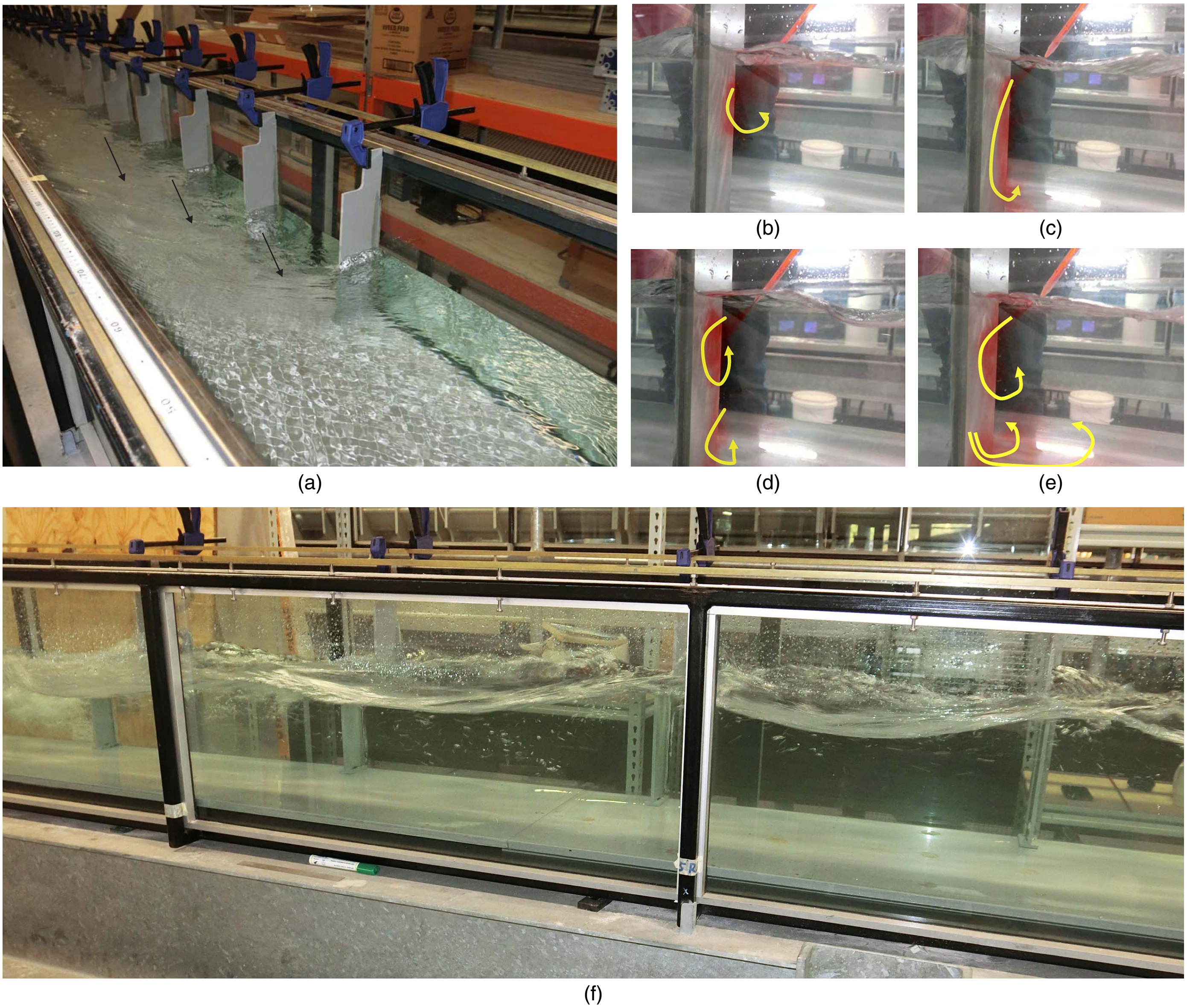

Fig. 3. Free-surface flow patterns in an open channel with full-height sidewall baffles: (a) free-surface flow pattern in an open channel with medium sidewall baffles $h_b = 0.083$ m, distance between baffles $L_b = 0.333$ m, flow rate $Q = 0.056$ m^3/s, and flow direction from bottom right to top left, with arrows pointing to cross waves; (b) turbulent structures behind a baffle visualized using dye injection with Flow pattern 1 with flow direction from left to right, $h_b = 0.083$ m, $L_b = 0.333$ m, $Q = 0.056$ m^3/s; (c) Flow pattern 2 with flow direction from left to right, $h_b = 0.083$ m, $L_b = 0.333$ m, $Q = 0.056$ m^3/s; (d) Flow pattern 3 with flow direction from left to right, $h_b = 0.083$ m, $L_b = 0.333$ m, $Q = 0.056$ m^3/s; (e) Flow pattern 4 with flow direction from left to right, $h_b = 0.083$ m, $L_b = 0.333$ m, $Q = 0.056$ m^3/s; and (f) unstable sloshing conditions with self-sustained free-surface resonance, with $Q = 0.102$ m^3/s, $B = 0.5$ m, $S_o = 0$, $h_b = 0.083$ m, $L_b = 0.67$ m, $d = 0.272$ m, and $V_{\text{mean}} = 0.76$ m/s (shutter speed $= 1/40$ s), and with flow direction from right to left.

pattern 3) [Fig. 3(d)]. The two plumes were then advected downstream by the main flow while rotating and dissipating by turbulent eddies in the flow (Flow pattern 4) [Fig. 3(e)]. This entire process confirmed the flow deceleration behind the baffle and the existence of turbulent coherent structures decaying from large to smaller scales.

Flow Resistance

Free-surface measurements were conducted to document the total flow resistance of the channel with and without plain sidewall baffles. For all flow conditions and baffle configurations, the free-surface elevation decreased with increasing longitudinal distance, corresponding to a steady H2 gradually varied flow backwater profile. The total flow resistance was derived from the free-surface profile data. The full data set is reported in Table 1 (last column). In presence of wall baffles, the channel flow resistance showed a marked increase compared with the smooth channel data (Fig. 4). Further, the data showed an increase in flow resistance with increasing discharge for a given configuration. That is, the flow resistance increased with decreasing aspect ratio B/d for a given baffle geometry (h_b, L_b). The data trend is seen in Fig. 4(a), in which the friction factor was inversely correlated to the aspect ratio B/d as follows:

$$f \propto \left(\frac{B}{d}\right)^{-0.52} \tag{2}$$

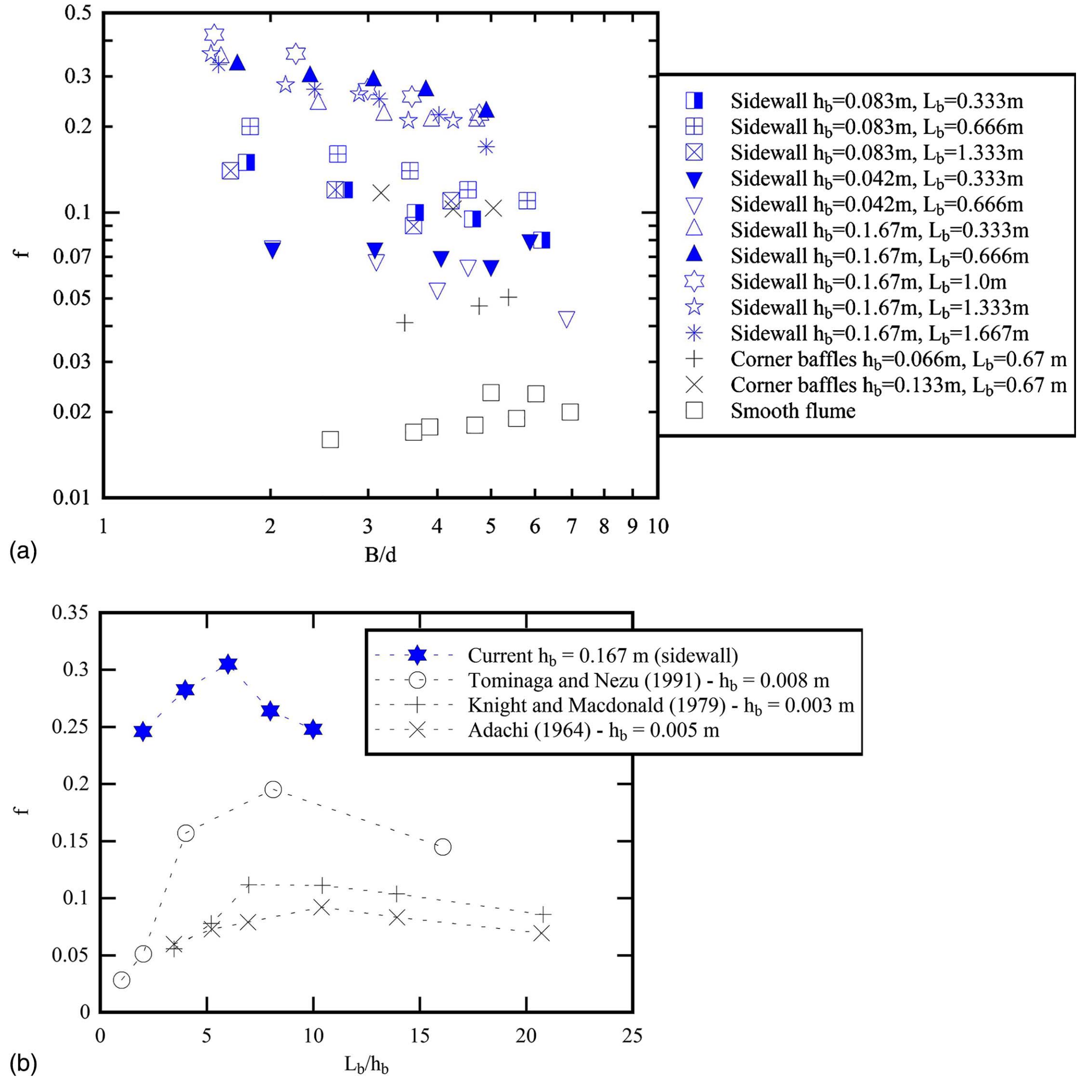

Fig. 4. Flow resistance in smooth and asymmetrical baffled channels: (a) flow resistance in smooth and asymmetrical baffled channels with Darcy-Weisbach friction factor as a function of the relative aspect ratio B/d, with dashed lines showing Eq. (2) for comparison between present data (sidewall baffles), asymmetrical triangular bottom baffle data (Cabonce et al. 2019), and smooth flume data (present data, Cabonce et al. 2019); and (b) effect of the relative longitudinal baffle spacing L_b/h_b on the flow resistance in a box culvert barrel equipped with asymmetrical wall baffles for $h_b = 0.167$ m for a comparison with the bottom rib experiments of Adachi (1964), Knight and Macdonald (1979), and Tominaga and Nezu (1991).

Although Eq. (1) showed a wider range of relevant dimensionless terms, the present data set implied a strong effect of the aspect ratio B/d and relative baffle size h_b/B on the flow resistance, with a lesser impact of the baffle spacing L_b/h_b.

The effect of the relative longitudinal spacing of sidewall baffles on the flow resistance was investigated for one baffle size, i.e., $h_b = 0.167$ m. The data are presented in Fig. 4(b), in which they are compared with some flow resistance data in open channels with bottom transverse bars. The current data showed a maximum in flow resistance for $L_b/h_b \sim 6$, with lesser flow resistance with shorter and longer baffle spacings. The finding was comparable to the literature with bottom cavity flows [Fig. 4(b)]. For such a longitudinal spacing, i.e., $L_b/h_b \sim 6$, a wake-interference regime was observed, and the flow became subjected to some complicated three-dimensional hydrodynamic motion (Roshko 1955; Perry et al. 1969). In particular, different lateral wake structures developed with the one-side-only baffle compared with those induced by bottom baffles of relatively small height, including with the development of large eddies with vertical axis.

Velocity and Boundary Shear Measurements

Longitudinal Velocity Field

Velocity measurements were conducted for the medium-sized baffles ($h_b = 0.083$ m and $L_b/h_b = 4$), at three longitudinal locations: $(x - x_b)/L_b = 0.05$, 0.5, and 0.75, where the longitudinal location of the reference baffle was $x_b = 8.20$ m, and x was measured from the upstream end of the flume. All velocity measurements were performed under a discharge of $Q = 0.054$ m^3/s.

Altogether, the data showed a significant effect of the baffles in decelerating the flow, evidenced by slower velocity at all elevations with transverse distance closer to the baffle (right sidewall) compared with the smooth channel data. The presence of baffles further changed the shape of velocity profile on the channel centerline, as illustrated in Fig. 5(a). The centerline velocity data on a smooth bed (no baffle) presented a partially developed boundary layer and a free-stream region above. With full-height sidewall baffles, the centerline velocity profiles showed a maximum velocity at

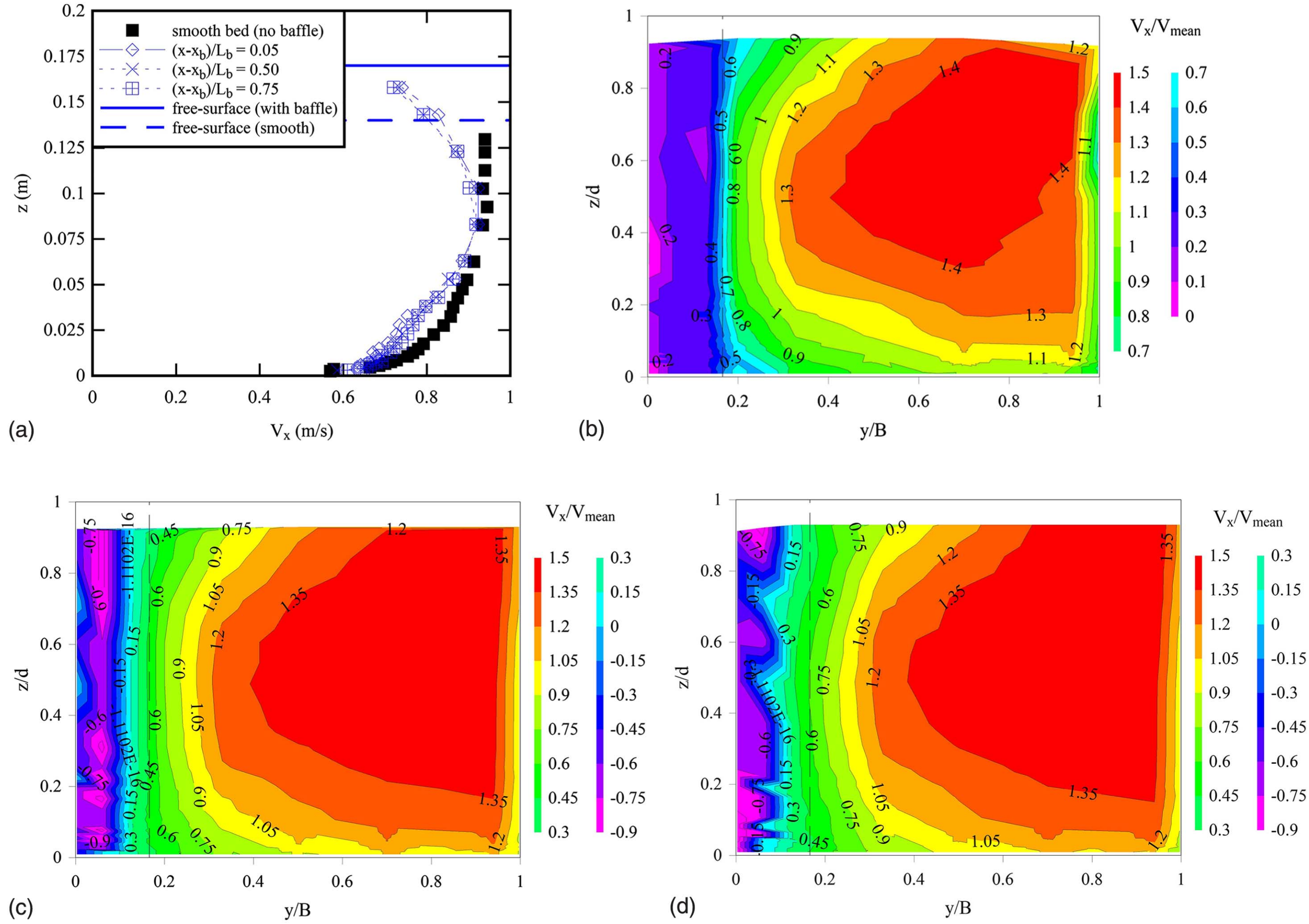

Fig. 5. Longitudinal velocities in the asymmetrical wall baffled channel for flow conditions $Q = 0.054\ \mathrm{m^3/s}$, $S_o = 0$, $h_b = 0.083$ m, $L_b = 0.33$ m, $x_b = 8.2$ m, and water depth $d = 0.17$ m measured at $x = 8$ m: (a) vertical profile of streamwise velocity on the channel centerline ($y = 0.25$ m) at dimensionless distances $(x - x_b)/L_b = 0.05$, 0.50, and 0.75 downstream of a medium baffle and on a smooth bed (no baffle); (b) velocity contour map at $(x - x_b)/L_b = 0.05$; (c) velocity contour map at $(x - x_b)/L_b = 0.5$; and (d) velocity contour map at $(x - x_b)/L_b = 0.75$.

approximately $z/d = 0.6$, with a decrease in velocity with increasing elevation for $0.6 < z/d < 1$. The baffled channel data presented a velocity dip next to the free surface, in addition to reduced centerline velocity, compared with the smooth channel for the same flow rate.

Some negative velocity was observed close to the baffled sidewall. Although a Prandtl-Pitot tube is not designed to measure flow velocity that is not directly opposing its tip, a lower reading in the dynamic tapping compared with the static tube was observed at these locations. Past experiments derived a correlation between the velocity and negative Pitot reading (Cabonce et al. 2019). Although the quantitative magnitude was questionable herein, the findings were qualitatively consistent with visual observations and dye injection. Whether such a negative velocity was strong enough to adversely impact on fish behavior (Cabonce et al. 2018) could be argued, and more detailed quantitative measurements would be required, e.g., using an acoustic Doppler velocimeter system.

Complete velocity contour maps are shown in Figs. 5(b–d), in which the edge of the wall baffles is shown with a vertical dashed line. The contour map included some interpolation between measurement points using the software DPlot version 2.3.5.7. Physically, the full-height wall baffles installed along the right sidewall induced a low-velocity zone for $0 < y/B < 0.167$. All the data showed an asymmetrical distribution of the streamwise velocity as a result of the presence of wall baffles. The high-velocity flow regions were shifted toward the left sidewall $0.6 < y/B < 0.9$, whereas a relatively large reduced-velocity zone was observed from the right sidewall to almost the center of the barrel channel $0 < y/B < 0.4$. Immediately behind the baffles, i.e., $0 < y/h_b < 1$ or $0 < y/B < 0.167$, the longitudinal velocities were very small and sometimes negative. The low-velocity zone behind baffles presented a good connectivity between two adjacent baffles because all measured cross sections showed similar areas and magnitudes of low-velocity regions [Figs. 5(b–d)].

Boundary Shear Stress

With the Prandtl-Pitot tube lying on a boundary, e.g., channel bed or sidewall, the boundary shear stress may be deduced from velocity data (Patel 1965; Cabonce et al. 2019). Fig. 6(a) presents the transverse distributions of boundary shear stress measured at three distances behind a baffle $(x - x_b)/L_b = 0.05$, 0.50, and 0.75. Herein, $(\tau_o)_{\mathrm{skin}}$ is the skin friction shear stress measured with the tube, $(\tau_o)_{\mathrm{total}} = f/8 \times \rho \times V_{\mathrm{mean}}^2$ is the total shear stress, with f the Darcy-Weisbach friction factor [Fig. 4(a)], V_{mean} the cross-sectional averaged velocity, and y' the perimetric coordinate defined following

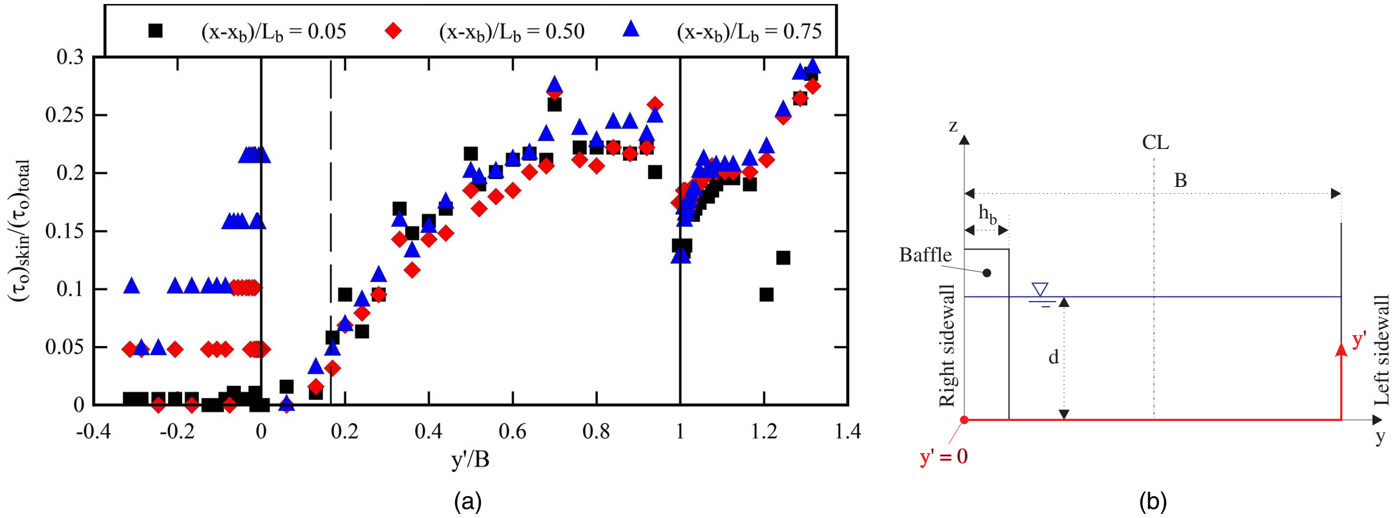

(a)

(b)

Fig. 6. Boundary shear stress distribution along the wetted perimeter of an asymmetrical wall baffle channel: (a) dimensionless skin friction shear stess $(\tau_o)_{\text{skin}}/(\tau_o)_{\text{total}}$ for $Q = 0.054\ \text{m}^3/\text{s}$, $S_o = 0$, $h_b = 0.083$ m, $L_b = 0.33$ m, $d = 0.17$ m (at $x = 8$ m), with solid lines marking the bottom corners and the dashed line corresponding to the outer edge of the full-height sidewall baffles; and (b) definition sketch of the perimetric coordinate y' looking upstream.

the wetted perimeter defined in Fig. 6(b). In Fig. 6(a), the vertical solid lines mark the bottom corners and transitions from bed measurements to sidewall measurements, with the dashed line marking the outer edge of the full-height sidewall baffles.

Overall, the boundary shear stress data showed an asymmetrical distribution induced by the baffles installed along the right wall. The finding was qualitatively consistent with the velocity data. Lower shear stress magnitudes were observed along the right (baffled) sidewall, compared with the channel bed and left sidewall. Along the channel bed, the transverse distribution of high shear stress was skewed toward the left sidewall. In terms of order of magnitudes, all three cross sections showed similar values and very comparable shape of shear stress distributions, with a substantially smaller skin friction shear stress than the total boundary shear stress.

The wetter-perimeter-averaged skin friction coefficient $\overline{f_{\text{skin}}}$ was calculated as follows:

$$\overline{f_{\text{skin}}} = \frac{8 \times \overline{(\tau_o)_{\text{skin}}}}{\rho \times V_{\text{mean}}^2} \tag{3}$$

where $\overline{(\tau_o)_{\text{skin}}}$ = wetter-perimeter-averaged boundary friction integrated along the entire wetted perimeter P_w

$$\overline{(\tau_o)_{\text{skin}}} = \frac{1}{P_w} \times \int_{P_w} (\tau_o)_{\text{skin}} \times dy' \tag{4}$$

The present results showed a small contribution (<15%) of the skin friction to the overall flow resistance (Table 2, ninth column). Table 2 summarizes the wetter-perimeter-averaged skin friction coefficient data. The current data were further compared with past physical studies in similar channels with comparable discharges, but with different boundary treatments (Table 2). The skin friction coefficients $\overline{f_{\text{skin}}}$ were of the same order of magnitude compared with smooth channel data, as well as to skin friction data in channels equipped with small bottom corners and sidewall rib. Altogether, the experimental results suggested an apparent boundary roughening of flow with the presence of asymmetrical wall baffles, for which the flow resistance was primarily form drag.

Discussion

A number of key findings may be derived from the velocity measurements conducted in the present study. These include (1) a strong flow asymmetry caused by the presence of full-height wall baffles in terms of both velocity and boundary shear stress distributions; (2) some sizable low-velocity regions that were well-connected behind and between wall baffles, likely conducive of upstream fish passage; (3) a significant reduction in skin friction boundary shear stress along the sidewall where baffles were installed; and (4) a sizeable negative velocity zone behind and close to the baffles.

With traditional bottom-mounted baffles and bottom-corner baffles, the impact of the baffles on the flow field and channel flow resistance decreases with increasing discharges for a given channel geometry and baffle dimensions (Engel 1974; Knight and Macdonald 1979; Cabonce et al. 2018). With full-height sidewall baffles, the trend differed significantly. Namely, the flow resistance increased with increasing flow depth, and hence discharge [Fig. 4(a)].

A few limitations in instrumentation will need to be addressed in future works, e.g., the inaccuracy in measuring the fluctuating free surface and the velocity measurements immediately behind the baffles. In addition, no turbulent fluctuations or negative recirculation were quantified in the present study, although both could affect the behavior and upstream migration of small-body-mass fish (Cabonce et al. 2018).

Conclusion

Physical modeling was conducted in a 0.5-m-wide box culvert barrel channel equipped with asymmetrical wall baffles. The measurements were performed for a broad range of discharges and baffle geometries, with the plain rectangular wall baffles installed along the right sidewall only, and a constant baffle size and spacing. The current study focused on a complete hydrodynamic characterization of the impact of wall baffles on a box culvert barrel equipped with wall baffles, although their impact on fish passage was not tested. The physical data delivered a fine characterization of the

Table 2. Wetted-perimeter-averaged skin friction coefficient f_{skin} for a smooth channel with sidewall baffles: comparison with past studies

References	Q (m^3/s)	B (m)	d^a (m)	$V_{\text{mean}}{}^a$ (m/s)	x (m)	$(x-x_b)/L_b$	$\overline{f_{\text{skin}}}$	f_{skin}/f	Configuration
Present study	0.054	0.50	0.17	0.6353	8.21	0.05	0.0153	0.127	Full-height sidewall baffles
					8.357	0.5	0.0165	0.137	($h_b = 0.083$ m and
					8.43	0.75	0.0191	0.159	$L_b = 0.333$ m), one side only
Cabonce et al. (2019)	0.0556	0.50	0.162	0.686	8	—	0.0145	1	Smooth channel
			0.1625	0.684			0.0102[b,c]	0.28[b,c]	Small plain corner baffles ($h_b = 0.067$ m and $L_b = 0.67$ m), one side only
			0.166	0.643			0.0128[b,c]	0.22[b,c]	Small plain corner baffles ($h_b = 0.133$ m and $L_b = 0.67$ m), one side only
Sanchez et al. (2020)	0.056	0.50	0.147	0.7831	8	—	0.0098	0.48	Sidewall square (50 mm) streamwise rib, one side only
Sailema et al. (2020)	0.0556	0.50	0.20	0.542	8	—	0.0193[b]	0.084[b]	Small plain corner baffles ($h_b = 0.133$ m and $L_b = 0.67$ m), both sides
			0.0199	0.55		—	0.0092[b]	0.048[b]	Small brush corner baffles ($h_b = 0.133$ m and $L_b = 0.67$ m), both sides
			0.197	0.564		—	0.0146[b]	0.064[b]	Small corner baffles with holes ($h_b = 0.133$ m and $L_b = 0.67$ m), both sides

Note: $\overline{f_{\text{skin}}}$ = cross-sectional averaged skin friction coefficient.
[a]Measured at $x = 8$ m.
[b]Longitudinal average over a full baffle spacing.
[c]Bed shear stress data only, excluding sidewall.

hydrodynamics of the asymmetrical baffled culvert barrel. The results showed a very significant impact of the asymmetrical wall baffles on the turbulent flow conditions in the culvert barrel. The observations indicated in particular a substantial increase in flow turbulence and flow resistance, as well as an asymmetrical turbulent velocity field.

The physical modeling data illustrated the drastic impact of a seemingly simple boundary treatment (plain rectangular baffles) on the flow field, even if the effect is lower for wider culvert barrels. In practice, the installation of baffles has practical implications, encompassing the installation costs, an increase in channel size to achieve the same design discharge and afflux, and regular maintenance and repairs after flood events, including removal of debris and sediments trapped by the baffles. The present physical results may serve as a validation data set for future computational fluid dynamics (CFD) modeling. Properly validated CFD modeling could assist with the development of more efficient baffle designs, although any optimum boundary treatment must closely target the relevant fish species.

Data Availability Statement

Some or all data, models, or code that support the findings of this study are available from the corresponding author upon reasonable request. These include the tabular data corresponding to the data presented in Figs. 4–6.

Acknowledgments

The authors thank Dr. Carlos Gonzalez (Queensland Department of Transport and Main Roads), Brady Zieth (Bechtel Australia), and Dr. Hang Wang (Sichuan University) for their comments on the original study. They further thank the anonymous reviewers for their detailed comments. They acknowledge the technical assistance of Jason Van Der Gevel and Stewart Matthews (University of Queensland). The financial support through the Queensland Department of Transport and Main Roads (TMTHF1805) is acknowledged.

Notation

The following symbols are used in this paper:

a = wave amplitude (m);
B = channel width (m);
D_H = hydraulic diameter (m);
d = water depth (m);
d_c = critical flow depth (m);
Fr = Froude number; for a rectangular channel, where $Fr = V/(g \times d)^{1/2}$;
f = Darcy-Weisbach friction factor;
$\overline{f_{\text{skin}}}$ = wetted perimeter averaged skin friction factor;
g = gravity acceleration (m/s^2), with $g = 9.794$ m/s^2 in Brisbane, Australia;
h_b = sidewall baffle height (m) measured from the right sidewall and triangular baffle height (m);
k_s = equivalent sand roughness height (m);
L_b = longitudinal spacing (m) between baffles;
L_t = turbulent length scale (m);
Mo = Morton number;
P = pressure (Pa);
P_w = wetted perimeter (m);
Q = water discharge (m^3/s);
Re = Reynolds number defined in terms of the hydraulic diameter, where $Re = \rho \times V_{\text{mean}} \times D_H/\mu$;

T_t = turbulent time scale (s);
V = velocity (m/s);
V_{mean} = cross-sectional mean velocity (m/s);
V_x = longitudinal velocity component (m/s);
x = longitudinal distance (m) positive downstream;
x_b = longitudinal baffle position (m);
y = transverse distance (m) measured from the right sidewall positive toward the left sidewall;
y' = transverse coordinate (m) following the wetted perimeter, with $y' = 0$ at the bottom right corner;
z = vertical distance (m) positive upwards, with $z = 0$ at the invert;
θ = angle between bed slope and horizontal;
μ = dynamic viscosity (Pa · s) of water;
ρ = water density (kg/m^3);
σ = surface tension (N/m) between air and water;
τ_o = boundary shear stress (Pa);
$(\tau_o)_{skin}$ = local skin friction boundary shear stress (Pa) measured with a Prandtl-Pitot tube lying on the boundary;
$\overline{(\tau_o)_{skin}}$ = wetted perimeter averaged skin friction boundary shear stress (Pa);
$(\tau_o)_{total}$ = total boundary shear stress (Pa); and
Ø = diameter (m).

Subscript

b = baffle characteristics;
c = critical flow conditions; and
1 = inflow conditions.

References

Adachi, S. 1964. *On the artificial strip roughness*, 20. Disaster Prevention Research Institute Bulletin, No. 69. Kyoto, Japan: Kyoto Univ.

Behlke, C. E., D. L. Kane, R. F. McLeen, and M. T. Travis. 1991. *Fundamentals of culvert design for passage of weak-swimming fish*. Rep. No. FHW A-AK-RD-90-10. Fairbanks, AK: Dept. of Transportation and Public Facilities.

Cabonce, J., R. Fernando, H. Wang, and H. Chanson. 2019. "Using small triangular baffles to facilitate upstream fish passage in standard box culverts." *Environ. Fluid Mech.* 19 (1): 157–179. https://doi.org/10.1007/s10652-018-9604-x.

Cabonce, J., H. Wang, and H. Chanson. 2018. "Ventilated corner baffles to assist upstream passage of small-bodied fish in box culverts." *J. Irrig. Drain. Eng.* 144 (8): 0418020. https://doi.org/10.1061/(ASCE)IR.1943-4774.0001329.

Cahoon, J. E., T. McMahon, A. Solcz, M. D. Blank, and O. Stein. 2007. *Fish passage in Montana culverts: Phase II—Passage goals*. Rep. No. FHWA/MT-07-010/8181. Washington, DC: Federal Highway Administration.

Chanson, H. 2004. *The hydraulics of open channel flow: An introduction.* 2nd ed., 630. Oxford, UK: Butterworth-Heinemann.

Chanson, H., and X. Leng. 2021. *Fish swimming in turbulent waters—Hydraulics guidelines to assist upstream fish passage in box culverts*. Leiden, Netherlands: Taylor & Francis Group.

Duguay, J., and R. W. J. Lacey. 2014. "Effect of fish baffles on the hydraulic roughness of slip-lined culverts." *J. Hydraul. Eng.* 141 (1): 04014065. https://doi.org/10.1061/(ASCE)HY.1943-7900.0000942.

Dynesius, M., and C. Nilsson. 1994. "Fragmentation and flow regulation of river systems in the northern third of the world." *Science* 266 (5186): 753–762. https://doi.org/10.1126/science.266.5186.753.

Engel, P. 1974. *Fish passage for culverts of the Mackenzie Highway*, 67. Burlington, Canada: Canadian Centre for Inland Waters.

Henderson, F. M. 1966. *Open channel flow*. New York: MacMillan.

Kapitzke, I. R. 2010. *Culvert fishway planning and design guidelines*. Townsville, Australia: James Cook Univ.

Kemp, P. 2012. "Bridging the gap between fish behaviour, performance and hydrodynamics: An ecohydraulics approach to fish passage research." *River Res. Appl.* 28: 403–406. https://doi.org/10.1002/rra.1599.

Knight, D. W., and J. A. Macdonald. 1979. "Hydraulic resistance of artificial strip roughness." *J. Hydraul. Div.* 105 (6): 675–690.

Larinier, M. 2002. "Fish passage through culverts, rock weirs and estuarine obstructions." *Bull. Fr. Pêche Pisciculture* 364: 119–134. https://doi.org/10.1051/kmae/2002097.

Leng, X., and H. Chanson. 2019. *Physical modelling of sidewall baffles in standard box culvert barrel to assist upstream fish passage*, 87. Hydraulic Model Rep. No. CH115/19. Brisbane, Australia: School of Civil Engineering, Univ. of Queensland.

Marsden, T. 2015. *Common rail proof of concept and baffle field trial assessment report.* Rep. No. OceanWatch Australia. St Ives Chase, NSW, Australia: Australasian Fish Passage Services.

Meile, T., J. L. Boillat, and A. J. Schleiss. 2011. "Water-surface oscillations in channels with axi-symmetric cavities." *J. Hydraul. Res.* 49 (1): 73–81. https://doi.org/10.1080/00221686.2010.534671.

Olsen, A., and B. Tullis. 2013. "Laboratory study of fish passage and discharge capacity in slip-lined, baffled culverts." *J. Hydraul. Eng.* 139 (4): 424–432. https://doi.org/10.1061/(ASCE)HY.1943-7900.0000697.

Patel, V. C. 1965. "Calibration of the Preston tube and limitations on its use in pressure gradients." *J. Fluid Mech.* 23 (1): 185–208. https://doi.org/10.1017/S0022112065001301.

Perry, A. E., W. H. Schofield, and P. N. Joubert. 1969. "Rough wall turbulent boundary layers." *J. Fluid Mech.* 37 (2): 383–413. https://doi.org/10.1017/S0022112069000619.

Preston, J. H. 1954. "The determination of turbulent skin friction by means of Pitot tubes." *J. R. Aeronaut. Soc.* 58 (518): 109–121. https://doi.org/10.1017/S0368393100097704.

Roshko, A. 1955. *Some measurements of flow in a rectangular cutout. NACA Technical Note 3488*. Pasadena, CA: California Institute of Technology.

Rouse, H. 1938. *Fluid mechanics for hydraulic engineers*. New York: McGraw-Hill.

Sailema, C., R. Freire, H. Chanson, and G. Zhang. 2020. "Modelling small ventilated corner baffles for box culvert barrel." *Environ. Fluid Mech.* 20 (2): 433–457. https://doi.org/10.1007/s10652-019-09680-2.

Sanchez, P. A., X. Leng, J. Von Brandis-Martini, and H. Chanson. 2020. "Hybrid modelling of low velocity zones in an asymmetrical channel with sidewall longitudinal rib to assist fish passage." *River Res. Appl.* 36 (5): 807–818. https://doi.org/10.1002/rra.3600.

Tominaga, A., and I. Nezu. 1991. "Turbulent structure past strip roughness in open channel flows." In *Proc., 24th IAHR Biennial Congress*, 42–50. Madrid, Spain: International Association for Hydro-Environment Engineering and Research.

Tuna, B. A., and D. Rockwell. 2014. "Self-sustained oscillations of shallow flow past sequential cavities." *J. Fluid Mech.* 758: 655–685. https://doi.org/10.1017/jfm.2014.548.

Yossef, M. F. M., and H. J. De Vriend. 2011. "Flow details near River Groynes: Experimental investigation." *J. Hydraul. Eng.* 137 (5): 504–516. https://doi.org/10.1061/(ASCE)HY.1943-7900.0000326.